論文 / 著書情報
Article / Book Information

Title	Elastic critical local buckling stress in cold-formed lipped channel and hat sections under uniform compression
Authors	Kazuya Mitsui, Kikuo Ikarashi, Tomoki Kobashi, Ryohei Kuwada
Citation	Thin-Walled Structures, Vol. 191, No. 111064,
Pub. date	2023, 8
DOI	https://dx.doi.org/10.1016/j.tws.2023.111064

Thin-Walled Structures 191 (2023) 111064

Contents lists available at ScienceDirect

Thin-Walled Structures

journal homepage: www.elsevier.com/locate/tws

Full length article

Elastic critical local buckling stress in cold-formed lipped channel and hat sections under uniform compression

Kazuya Mitsui [a,*], Kikuo Ikarashi [a], Tomoki Kobashi [b], Ryohei Kuwada [c]

[a] School of Environment and Society, Tokyo Institute of Technology, M1-43, 2-12-1 Ookayama, Meguro, Tokyo 152-8550, Japan
[b] Department of Architecture, Chiba Institute of Technology, 2-17-1 Tsudanuma, Narashino, Chiba 275-0016, Japan
[c] Steel Structures Research Laboratory, Nippon Steel Corporation, 20-1 Shintomi, Futtsu, Chiba 293-8511, Japan

ARTICLE INFO

Keywords:
Lipped channel section
Hat section
Local buckling
Plate element interaction
Energy method

ABSTRACT

The classical design approach for the elastic critical local buckling load of the cold-formed open section (CFOS) neglects the plate element interaction at the cross-section, which compromises the benefits of CFOSs designed for high performance. To derive a novel formula for the local buckling coefficient, taking into account the plate element interaction at the cross-section, a series of displacement functions for expressing the buckling deformations of the web, flanges, and lips caused by local buckling in CFOSs is proposed in this paper. The effect of cross-sectional geometry on the buckling coefficient was investigated using the proposed formula derived from Timoshenko's plate buckling theory. Further, simplified formulae were proposed for the buckling coefficient and half wavelength of the elastic critical local buckling for practical use. The reliabilities of the proposed formulae were verified by comparing the results obtained from the proposed formulae with the analysis results based on the finite element method and finite strip method.

1. Introduction

Cold-formed open sections (CFOSs) such as thin-walled lipped channel and hat sections can deliver high performance with a small quantity of steel and are rapidly becoming popular owing to their ease of fabrication. The utilization of high-strength steel and development of low-cost products in recent manufacturing processes has further improved the structural performance of CFOSs. However, CFOSs are characterized by low thickness and are therefore prone to multiple patterns of instability phenomena, such as local, distortional, and flexural buckling at low stress levels. The values of the buckling load vary in a complicated manner depending on the cross-sectional geometry. Accordingly, to maximize the performance, the member design must be based on a design formula that can accurately calculate the buckling load. Therefore, since 2007, the North American Specifications for the Design of Cold-Formed Steel Structures [1] have suggested a computational design method known as the direct strength method (DSM) [2] to manage such instability problems. The DSM allows the use of relatively simple-to-handle tools, such as the finite strip method (FSM) [3], which can analyze the elastic critical stresses of local, distortional, and flexural buckling. The most significant advantage of the FSM is that the boundary conditions at the plate-to-plate junctures are reflected in the elastic critical stresses, and the plate element interaction is considered. Therefore, the ultimate load of the CFOS can be determined based on accurately calculated critical buckling stresses. Nevertheless, some engineers prefer to use traditional simple design formulae for elastic critical buckling loads as opposed to analytical methods. Thus, in recent decades, scholars have investigated the influence of plate element interactions and proposed closed-form formulae for the elastic critical local buckling load.

The classical design method for the elastic critical local buckling load of the CFOS involves the evaluation of the buckling coefficient for each plate by neglecting the plate element interaction at the cross-section and considering the minimum value as the elastic critical local buckling load, which is incorporated into the American Iron and Steel Institute (AISI) specifications [1] and other current codes and specifications [4,5]. However, the design approach of neglecting the plate element interaction compromises the benefits of CFOSs designed for high performance. Accordingly, design formulae and computational approaches were derived for local buckling by considering the plate element interaction. Schafer and Peköz [6] presented the closed-form formulae for local and distortional buckling under compression. The formulae for local buckling accounted for the interaction between the connected plates because they were derived based on FSM results. Schafer [7] also provided semi-empirical formulae for local buckling

Abbreviations: CFOS, Cold-formed open section; DSM, Direct strength method; FEM, Finite element method; FSM, Finite strip method

* Corresponding author.
E-mail addresses: mitsui.k.ad@m.titech.ac.jp (K. Mitsui), ikrashi.k.aa@m.titech.ac.jp (K. Ikarashi), kobashi.tomoki@p.chibakoudai.jp (T. Kobashi), kuwada.r6a.ryohhei@jp.nipponsteel.com (R. Kuwada).

https://doi.org/10.1016/j.tws.2023.111064
Received 10 April 2023; Received in revised form 21 July 2023; Accepted 27 July 2023
Available online xxxx
0263-8231/

in bending, which were determined by fitting FSM results. Kobashi et al. [8,9] focused on the restraining effects of plate element interactions on local buckling of rectangular-box-section members and theoretically derived design formulae. They stated that the width-to-thickness ratio has no effect on the buckling coefficient of local buckling if the thickness of the plates constituting the cross-section is uniform. Yu and Schafer [10] studied the effect of moment gradients on the buckling stress of thin-walled sections based on the Rayleigh–Ritz solution that included an assumed deflection function as a combination of a polynomial and trigonometric series. Kimura et al. [11] investigated the plate element interaction of I-shaped beam cantilevers and proposed formulae for the elastic local buckling strength of each plate based on the energy method. To simulate the complex boundary conditions of each plate, trigonometric functions that captured the behavior of the plates were utilized in the energy method. They reported that boundary conditions for each plate varied between the pinned and fixed boundary conditions. Mitsui and Ikarashi [12] used the energy method to investigate the boundary condition of the web-flange junctures in cold-formed lipped channel members. They concluded that the boundary conditions of the web in the lipped channel members are intermediate between simple and fixed conditions. Salles et al. [13] presented a method for decomposing the general deformation shape of a lipped channel column into three main buckling modes – local, distortional, and flexural global – and derived the buckling load of each buckling mode based on the energy approach. The cubic polynomials used in the FSM were employed to describe the cross-sectional deformation of local buckling in their study. This is because the accurate computation of the elastic critical buckling load requires displacement functions that can correctly reproduce the buckling deformation occurring in the cross-section. Lu et al. [14] investigated the effects of end-boundary conditions on the local buckling load of a CFOS in a stub column. They proposed a theoretical analysis model that reflected the plate element interaction between the flanges and lips on the web by considering rotational springs to derive explicit formulae for the local buckling load. In addition to these theoretical studies, several experimental and analytical investigations of plate element interaction have been conducted [15–24]. Based on the contributions of these studies, the elastic local buckling load can be derived with greater accuracy when compared with the result obtained using the conventional design approach.

In the classical design approach, the elastic critical local buckling stress of the plate is determined using Eq. (1).

$$\sigma_{cr} = k\frac{\pi^2 E}{12\left(1-\nu^2\right)}\left(\frac{t}{b}\right)^2, \tag{1}$$

where σ_{cr} is the elastic critical buckling stress, E is the modulus of elasticity, ν is the Poisson's ratio, t is the thickness, and b is the width of the plate. k is the buckling coefficient, which varies with the cross-sectional geometry, boundary, and loading conditions. In general, the buckling coefficient of a simply supported plate, which has the lowest value, is employed as a conservative measure [5]. However, the actual boundary condition of each plate is expected to be within the range of the simply supported and fixed support conditions, as reported in previous studies [7,8,11–13]. In other words, the member design procedure based on the minimum buckling coefficient does not optimize the cross-sectional geometry of CFOS, thereby failing to harness its full performance potential. To address these shortcomings, this study focuses on the elastic critical local buckling load of CFOSs, such as the thin-walled lipped channel sections and hat sections shown in Fig. 1, under uniform compression. In particular, a novel formula is derived for the buckling coefficient; the formula yields almost the same values as obtained by the FSM and finite element method (FEM) analyses in a theoretical solution. To accomplish this task, displacement functions that can accurately capture the deformation due to local buckling under uniform compression of each plate comprising the cross-section are proposed. This is described in Section 2. Then, a theoretical

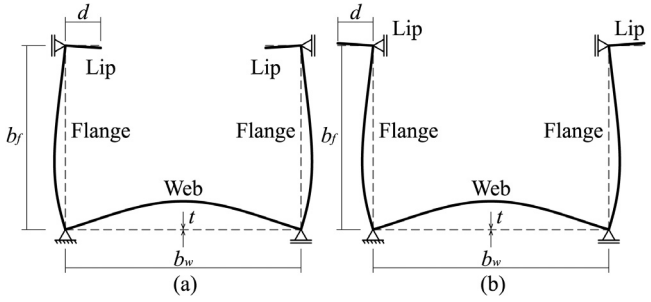

Fig. 1. Deformed shape of local buckling: (a) Lipped channel section. (b) Hat section.

analysis is performed using the proposed displacement functions and the energy approach based on Timoshenko's plate buckling theory [25]. The effect of the cross-sectional geometry on the elastic critical local buckling stress is discussed in Section 3. During the discussion of the theoretical analysis, four shape ratios related to the member profile are defined [length-to-width ratio of the web ($\lambda_w = L/b_w$), web-to-flange width ratio ($\chi_f = b_f/b_w$), web-to-lip width ratio ($\chi_l = d/b_w$), and width-to-thickness ratio of the web ($\chi_t = b_w/t$), where L is the column length, b_w is the depth of the web, b_f is the width of the flange, and d is the width of the lip]. Furthermore, it is theoretically shown that only three shape ratios (λ_w, χ_f, and χ_l) are related to the buckling coefficient for the elastic critical local buckling. Finally, a closed-form simplified formula for the elastic critical local buckling coefficient and a formula for the critical half-wavelength ratio that minimizes the elastic critical local buckling stress are presented. The validity of the proposed formulae is examined through comparison with the results of parametric FEM analysis and the cross-section elastic buckling analysis (CUFSM) software [26].

2. Derivation of elastic critical local buckling coefficient

2.1. Proposed displacement functions for local buckling

Fig. 2(a) shows an overview of the model and coordinate system applied in the theoretical analysis. A cold-formed lipped channel section is considered as an example. The thickness is assumed to be constant for the entire member, and each plate remains orthogonal after local buckling, where the bent portions between the plate elements were ignored. A CFOS buckles locally with several half-waves along the member length when subjected to uniform compression. Fig. 2(b) shows the cross-sectional deformation of the CFOS at an arbitrary z-coordinate.

In this study, the elastic critical local buckling load was derived based on Timoshenko's plate buckling theory [26], which requires setting up displacement functions for each plate forming the cross-section as well as consideration of the plate element interaction to obtain an accurate calculation of the local buckling stress. According to the coordinate system defined in Fig. 2(a) and (b), the deformed shape of the web, flanges, and lips due to local buckling can be expressed by multiplying the deformation in the longitudinal direction by that in the width direction of each plate as follows:

$$w_w(y,z) = u(z)\,w(y), \tag{2a}$$

$$w_f(x,z) = u(z)\,f(x), \tag{2b}$$

$$w_l(y,z) = u(z)\,l(y), \tag{2c}$$

where $w_w(y, z)$, $w_f(x, z)$, and $w_l(y, z)$ are the displacement functions of the web, flange, and lip, respectively; the functions $w(y)$, $f(x)$, and $l(y)$ represent the cross-sectional deformation of each plate, and $u(z)$ represents the deformation in the longitudinal direction. The form of the displacement function varies depending on the boundary conditions

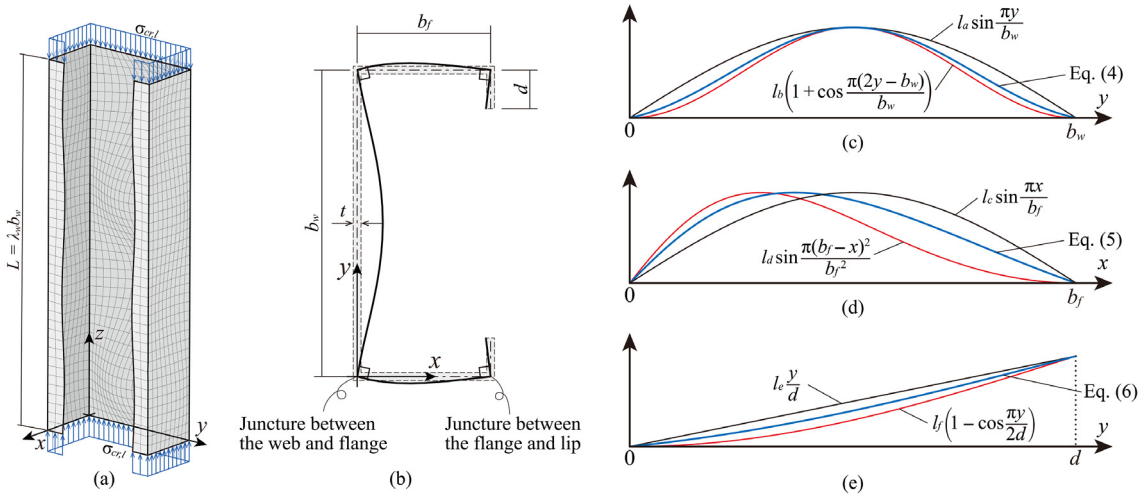

Fig. 2. Local buckling deformation of the CFOS: (a) Theoretical analysis model and coordinate system (e.g., lipped channel member). (b) Cross-sectional deformation. (c) Displacement function of the web. (d) Displacement function of the flange. (e) Displacement function of the lip.

at the plate ends. It can be expressed using Eq. (3a) for the simple support condition and Eq. (3b) for the fixed support condition.

$$u(z) = \sin\frac{m\pi z}{L}, \tag{3a}$$

$$u(z) = \sin\frac{\pi z}{L}\sin\frac{m\pi z}{L}, \tag{3b}$$

where m denotes the number of buckling half-waves along the longitudinal direction. Because the web is joined to flanges and lips of the same shape, the deformation of the web can be assumed to be line symmetric. Subsequently, the following function is adopted for the cross-sectional deformation of the web:

$$w(y) = l_a \sin\frac{\pi y}{b_w} + l_b\left(1+\cos\frac{\pi\left(2y-b_w\right)}{b_w}\right), \tag{4}$$

where l_a and l_b are constants that determine the deformed shape of the web. Fig. 2(c) shows the functions of Eq. (4). In earlier studies [8,11–14], the boundary condition for a plate with other plates joined to it on both edges was reported to be in the range between the conditions of simple and fixed supports; thus, Eq. (4) is expressed as a combination of sinusoidal and cosine waves. In contrast, it can be assumed that the flanges are joined to the web and lip of different widths and that the boundary conditions at both edges are different, resulting in a nonlinear symmetric deformation. The following function was proposed for the cross-sectional deformation of the flanges:

$$f(x) = l_c \sin\frac{\pi x}{b_f} + l_d \sin\frac{\pi\left(b_f-x\right)^2}{b_f^2}, \tag{5}$$

where l_c and l_d denote constants that determine the shape of the deformed flange. As shown in Fig. 2(d), Eq. (5) consists of a combination of a sinusoidal function and a non-line-symmetric function. Finally, Eq. (6) is adopted for the cross-sectional deformation of the lip.

$$l(y) = l_e\frac{y}{d} + l_f\left(1-\cos\frac{\pi y}{2d}\right), \tag{6}$$

where l_e and l_f are constants that determine the deformed shapes of the lips. When the lip width is relatively small, it can be assumed that the lip is nearly rigid and its out-of-plane bending deformation decreases; however, when the lip width is relatively large, the lip deforms flexibly. Therefore, Eq. (6) can be expressed as a combination of functions, as shown in Fig. 2(e). Assuming that each plate retains the original angle at the junctures after local buckling, these displacement functions need to satisfy the following conditions in arbitrary z-coordinates: $\partial w/\partial y|_{y=0} = \partial f/\partial x|_{x=0}$ and $\partial f/\partial x|_{x=b_f} = \partial l/\partial y|_{y=0}$. Based on these conditions, each constant has the following relationships:

$$l_a = -b_w\left(l_c+2l_d\right)/b_f, \tag{7}$$

$$l_e = \pi d l_c/b_f. \tag{8}$$

As the cross-sectional geometry of the hat section is simply the reverse of the direction of the lip of the lipped channel section, Eqs. (2)–(8) can also be adopted for the buckling deformation of the hat members.

2.2. Strain energy and work performed by uniform compression

According to the energy method, the incremental strain energy for each plate can be expressed as

$$\Delta U_1 = \frac{D}{2}\int_0^L\int_0^{b_w}\left[\left(\frac{\partial^2 w_w}{\partial y^2}\right)^2+\left(\frac{\partial^2 w_w}{\partial z^2}\right)^2+2\nu\frac{\partial^2 w_w}{\partial y^2}\frac{\partial^2 w_w}{\partial z^2} +2(1-\nu)\left(\frac{\partial^2 w_w}{\partial y\partial z}\right)^2\right]dydz, \tag{9}$$

$$\Delta U_2 = \frac{D}{2}\int_0^L\int_0^{b_f}\left[\left(\frac{\partial^2 w_f}{\partial x^2}\right)^2+\left(\frac{\partial^2 w_f}{\partial z^2}\right)^2+2\nu\frac{\partial^2 w_f}{\partial x^2}\frac{\partial^2 w_f}{\partial z^2} +2(1-\nu)\left(\frac{\partial^2 w_f}{\partial x\partial z}\right)^2\right]dxdz, \tag{10}$$

$$\Delta U_3 = \frac{D}{2}\int_0^L\int_0^{d}\left[\left(\frac{\partial^2 w_l}{\partial y^2}\right)^2+\left(\frac{\partial^2 w_l}{\partial z^2}\right)^2+2\nu\frac{\partial^2 w_l}{\partial y^2}\frac{\partial^2 w_l}{\partial z^2} +2(1-\nu)\left(\frac{\partial^2 w_l}{\partial y\partial z}\right)^2\right]dydz, \tag{11}$$

where ΔU_1, ΔU_2, and ΔU_3 represent the strain energy of a single plate for the web, flange, and lip, respectively; L denotes the column length; $D = Et^3/[12(1-\nu^2)]$ denotes the flexural rigidity of the plate; E denotes the modulus of elasticity; and ν denotes Poisson's ratio. The incremental work performed by the uniform compression of the web, flange, and lip can be derived as

$$\sigma_{cr,l}\cdot\Delta T_1 = \frac{t\sigma_{cr,l}}{2}\int_0^L\int_0^{b_w}\left(\frac{\partial w_w}{\partial z}\right)^2 dydz = \frac{tk_{w,l}\sigma_0}{2}\int_0^L\int_0^{b_w}\left(\frac{\partial w_w}{\partial z}\right)^2 dydz, \tag{12}$$

$$\sigma_{cr,l}\cdot\Delta T_2 = \frac{t\sigma_{cr,l}}{2}\int_0^L\int_0^{b_f}\left(\frac{\partial w_f}{\partial z}\right)^2 dxdz = \frac{tk_{w,l}\sigma_0}{2}\int_0^L\int_0^{b_f}\left(\frac{\partial w_f}{\partial z}\right)^2 dxdz, \tag{13}$$

$$\sigma_{cr,l}\cdot\Delta T_3 = \frac{t\sigma_{cr,l}}{2}\int_0^L\int_0^{d}\left(\frac{\partial w_l}{\partial z}\right)^2 dydz = \frac{tk_{w,l}\sigma_0}{2}\int_0^L\int_0^{d}\left(\frac{\partial w_l}{\partial z}\right)^2 dydz, \tag{14}$$

where ΔT_1, ΔT_2, and ΔT_3 represent the work performed by uniform compression on a single plate of the web, flange, and lip, respectively; $\sigma_{cr,l}$ denotes the elastic critical stress for local buckling; $k_{w,l}$ is the buckling coefficient of the web that minimizes the elastic critical local buckling stress $\sigma_{cr,l} = k_{w,l}\sigma_0$; and σ_0 is the base stress defined to simplify the expression in this paper, as presented in Eq. (15).

$$\sigma_0 = \frac{\pi^2 E t^2}{12\left(1-\nu^2\right) b_w^2} \tag{15}$$

Assuming that the sum of the strain energy is equal to the sum of the work done by uniform compression, the potential energy Π can be obtained by performing an integral calculation as

$$\Pi = \Delta U_1 + 2\Delta U_2 + 2\Delta U_3 - k_{w,l}\sigma_0\left(\Delta T_1 + 2\Delta T_2 + 2\Delta T_3\right) = 0. \tag{16}$$

Based on the principle of minimum potential energy, an analytical formula can be obtained by differentiating Eq. (16) with respect to the auxiliary variables l_b, l_c, l_d, and l_f ($m = 1, 2, 3, \ldots$) as follows:

$$\begin{pmatrix} s_1 - e_1 k_{w,l,\mathrm{AF}} & s_2 - e_2 k_{w,l,\mathrm{AF}} & s_3 - e_3 k_{w,l,\mathrm{AF}} & s_4 - e_4 k_{w,l,\mathrm{AF}} \\ s_2 - e_2 k_{w,l,\mathrm{AF}} & s_5 - e_5 k_{w,l,\mathrm{AF}} & s_6 - e_6 k_{w,l,\mathrm{AF}} & s_7 - e_7 k_{w,l,\mathrm{AF}} \\ s_3 - e_3 k_{w,l,\mathrm{AF}} & s_6 - e_6 k_{w,l,\mathrm{AF}} & s_8 - e_8 k_{w,l,\mathrm{AF}} & s_9 - e_9 k_{w,l,\mathrm{AF}} \\ s_4 - e_4 k_{w,l,\mathrm{AF}} & s_7 - e_7 k_{w,l,\mathrm{AF}} & s_9 - e_9 k_{w,l,\mathrm{AF}} & s_{10} - e_{10} k_{w,l,\mathrm{AF}} \end{pmatrix} \begin{pmatrix} l_b \\ l_c \\ l_d \\ l_f \end{pmatrix} = 0, \tag{17}$$

where $k_{w,l,\mathrm{AF}}$ is the buckling coefficient determined by the analytical formula presented in Eq. (17). The elastic critical buckling stress for local buckling $\sigma_{cr,l,\mathrm{AF}} = k_{w,l,\mathrm{AF}}\sigma_0$ can be obtained by determining the lowest eigenvalues when Eq. (17) has nontrivial solutions, that is, when $(l_b\ l_c\ l_d\ l_f)^{\mathrm{T}}$ in Eq. (17) has a non-{0} solution. The buckling displacement corresponding to the elastic critical buckling stress is obtained as an eigenvector corresponding to the eigenvalues. The functions s_1, s_2, s_3, …, s_{10} and e_1, e_2, e_3, …, e_{10} in Eq. (17) are introduced to obtain Eq. (17) in a compact version. The process for deriving each function is described in Appendix. Considering a simply supported condition as an example, the components in Eq. (17) are expressed as shown below.

$$e_1 = 1.5 \tag{18a}$$

$$s_1 = 1.5\left(\frac{m}{\lambda_w}\right)^2 + 8\left(\frac{\lambda_w}{m}\right)^2 + 4 \tag{18b}$$

$$e_2 = -\frac{8}{3\pi\chi_f} \tag{18c}$$

$$s_2 = e_2\left(\frac{m}{\lambda_w} + \frac{\lambda_w}{m}\right)^2 \tag{18d}$$

$$e_3 = 2e_2 \tag{18e}$$

$$s_3 = 2s_2 \tag{18f}$$

$$e_4 = s_4 = e_9 = s_9 = 0 \tag{18g}$$

$$e_5 = \frac{3 + 6\chi_f^3 + 4\pi^2\chi_l^3}{6\chi_f^2} \tag{18h}$$

$$s_5 = \frac{1}{6\chi_f^2}\left\{3\left(\frac{m}{\lambda_w} + \frac{\lambda_w}{m}\right)^2 + 6\chi_f\left(\frac{m\chi_f}{\lambda_w} + \frac{\lambda_w}{m\chi_f}\right)^2 + 4\chi_l\left[\left(\frac{m\pi\chi_l}{\lambda_w}\right)^2 + 6(1-\nu)\right]\right\} \tag{18i}$$

$$e_6 = \frac{1 + 0.770\chi_f^3}{\chi_f^2} \tag{18j}$$

$$s_6 = \frac{\left(\frac{m}{\lambda_w} + \frac{\lambda_w}{m}\right)^2 + 0.770\chi_f\left(\frac{m\chi_f}{\lambda_w} + \frac{\lambda_w}{m\chi_f}\right)^2}{\chi_f^2} \tag{18k}$$

$$e_7 = \frac{\chi_l^2\left(\pi^2 - 4\pi + 8\right)}{\pi\chi_f} \tag{18l}$$

$$s_7 = e_7\left(\frac{m}{\lambda_w}\right)^2 + \frac{4 - (\pi+2)\nu}{\pi\chi_f} \tag{18m}$$

$$e_8 = \frac{2\left(1 + 0.378\chi_f^3\right)}{\chi_f^2} \tag{18n}$$

$$s_8 = \frac{2}{\chi_f^2}\left\{\left(\frac{m}{\lambda_w} + \frac{\lambda_w}{m}\right)^2 + 0.378\chi_f\left[\left(\frac{m\chi_f}{\lambda_w}\right)^2 + 5.00\left(\frac{\lambda_w}{m\chi_f}\right)^2 + 3.38\right]\right\} \tag{18o}$$

$$e_{10} = \frac{(3\pi - 8)\chi_l}{\pi} \tag{18p}$$

$$s_{10} = e_{10}\left(\frac{m}{\lambda_w}\right)^2 + \frac{1}{2\pi\chi_l}\left[\frac{\pi}{8}\left(\frac{\lambda_w}{m\chi_l}\right)^2 - 4\nu + \pi\right] \tag{18q}$$

As shown in Eqs. (17) and (18), the elastic critical local buckling stress of the CFOS is expressed as a function of the buckling coefficient of the web, $k_{w,l}$, which varies only with the integral constants shown in Eqs. (18a)–(18q). Moreover, Eqs. (18a)–(18q) are composed of only the three shape factors defined in this study [length-to-width ratio of the web ($\lambda_w = L/b_w$), web-to-flange width ratio ($\chi_f = b_f/b_w$), and web-to-lip width ratio ($\chi_l = d/b_w$)] and the material constants E and ν. That is, Eqs. (18a)–(18q) imply that the buckling coefficient of the elastic critical local buckling of the CFOS is affected only by the changes in the three shape factors. Note that the fourth column and fourth row of the matrix in Eq. (17) contain terms related to the flexible lips (out-of-plane deflection of the lip). Therefore, for a rigidly deformed lip (where it rotates around the flange-to-lip juncture without out-of-plane deformation), neglecting these terms and transforming the matrix to a 3 × 3 square form yield the elastic critical local buckling load. Moreover, as previously mentioned, the displacement function proposed for a lipped channel section can also be applied to a hat section. That is, the local buckling load of the lipped channel sections and hat sections can be obtained using the formulae shown in Eqs. (17) and (18).

Fig. 3 shows examples of the effect of the length-to-width ratio of the web λ_w on the elastic critical local buckling loads obtained using the derived analytical formula, assuming that the boundary condition at the plate end edges was a simple or fixed support. The elastic critical local buckling loads obtained through the FEM analysis and CUFSM [26] were compared with the calculation results obtained from the proposed analytical formula. Regarding the material properties, the modulus of elasticity E and Poisson's ratio ν were set to 205 GPa and 0.3, respectively. The details of the finite element (FE) model are presented in Section 4. The elastic critical local buckling loads were converted to the buckling coefficients $k_{w,l,\mathrm{AF}}$ (obtained from the proposed analytical formula), $k_{w,l,\mathrm{FEM}}$ (obtained from the FEM analysis), and $k_{w,l,\mathrm{CUFSM}}$ (obtained from CUFSM). The local buckling modes obtained from each method for the simple and fixed support conditions are shown in Fig. 4. As depicted in Fig. 3, the calculated elastic critical local buckling load obtained from the proposed formula agreed well with the predicted results obtained using the FEM analysis and CUFSM, regardless of the cross-sectional geometry. In addition, the buckling deformation and number of half-waves obtained by each method (Fig. 4) were the same. Therefore, the elastic critical local buckling load and buckling deformation can be estimated using the proposed analytical formula regardless of whether the lip extends in the inside or outside direction along the y-axis. Further validation of the derived analytical formula is presented in Section 4. As illustrated in Fig. 3, for web ratios below 5.0, the buckling coefficient of the elastic critical local buckling of the CFOS is influenced by the length-to-width ratio of the web. Nonetheless, as the length-to-width ratio of the web increases, the influence on the buckling coefficient diminishes and becomes negligible. Here, Fig. 3(a)

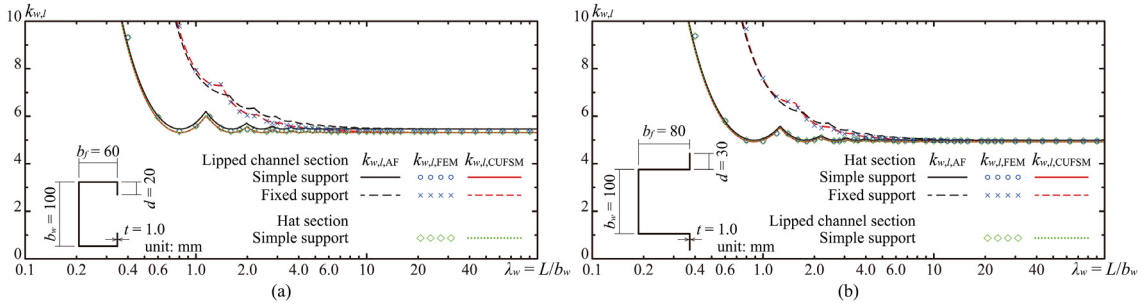

Fig. 3. Comparison of various signature local buckling loads: (a) Lipped channel section. (b) Hat section.

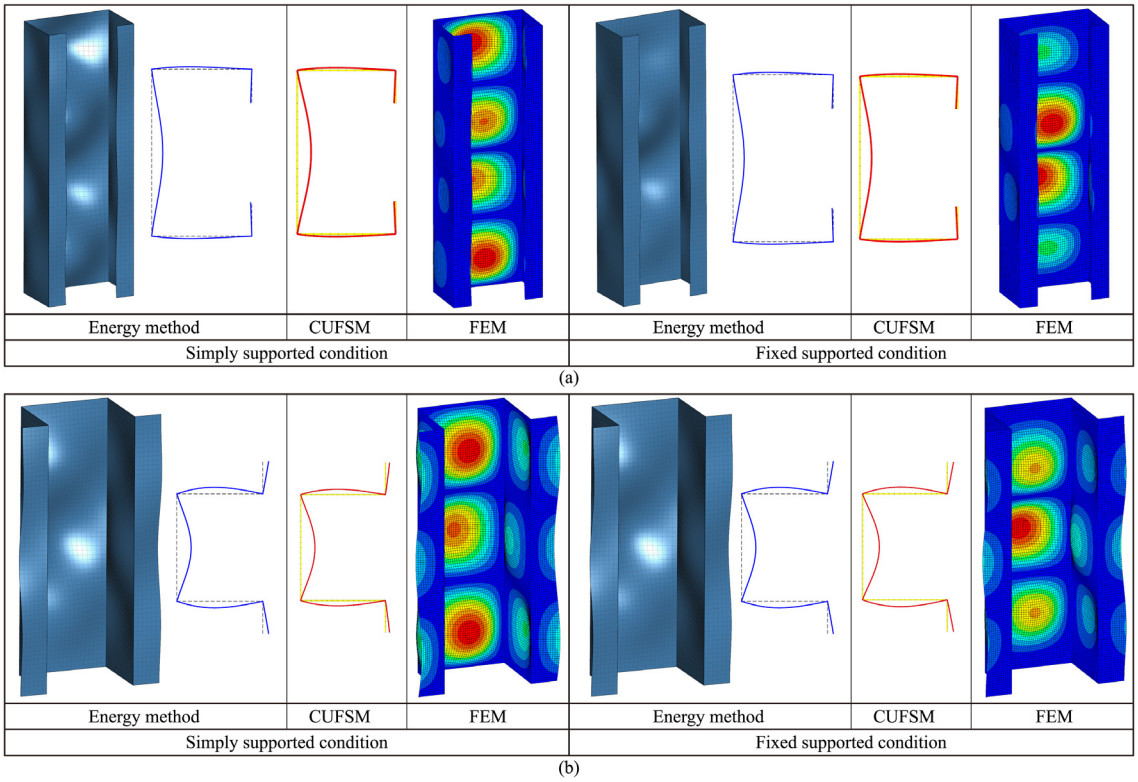

Fig. 4. Comparison of local buckling modes with $\lambda_w = 3$: (a) Lipped channel section (C-100 × 60 × 20 × 1.0). (b) Hat section (Hat −100 × 80 × 30 × 1.0).

shows the analytical results for the lipped channel section and results for the hat section with the same dimensions with simple support conditions. As shown in Fig. 3, if the cross-sectional dimensions are the same, the lipped channel and hat sections have the same local buckling stresses because the direction of only the lip is reversed. Therefore, the following discussion focuses on the lipped channel section.

3. Influence of cross-sectional geometry on local buckling coefficient

As shown in Fig. 3, the influence of the boundary conditions on the value of $k_{w,l}$ is significant when λ_w is less than 1.0, and the value of $k_{w,l}$ is higher for fixed support than for simple support. In contrast, the difference in the buckling coefficient decreases as the value of λ_w increases; furthermore, the convergence value (the minimum elastic critical load) of $k_{w,l}$ for each boundary condition is the same. In general, for most practical lengths of structural members, the length-to-width ratio of the web is larger than 3.0 [5], and the influence of the boundary conditions becomes relatively small. Therefore, by investigating the convergence value of $k_{w,l}$, it is possible to conservatively evaluate the buckling load and analyze the local buckling behavior of the CFOS. Based on the analytical equation for the simple support condition shown in Eqs. (17) and (18), we clarify the effect of the cross-sectional geometry on the convergence value of the local buckling coefficient for the CFOS.

The results shown in Fig. 5 were obtained from a parametric investigation of the convergence values of $k_{w,l,\mathrm{AF}}$ by using the proposed analytical formula for the simple support condition. The results obtained considering the flexible lips (out-of-plane deflection of the lips) are illustrated by black lines, and the results obtained by ignoring the out-of-plane deflection of the lips (rigid lips) are illustrated by red lines. First, it can be clearly seen that the web-to-flange width ratio $\chi_f = b_f/b_w$ is a dominant factor for the buckling coefficient in local buckling. The influence of the web-to-flange width ratio is shown in Fig. 6(a). As the web-to-flange width ratio increased, the values of $k_{w,l,\mathrm{AF}}$ decreased. When the web-to-flange ratio exceeded approximately 1.0, the values of $k_{w,l,\mathrm{AF}}$ became lower than 4.0. Because the minimum buckling coefficient of a plate with simple support conditions under uniform compression is 4.0, a web buckling coefficient of less than 4.0 implies that plates other than the web buckle locally. Examples of the cross-sectional shapes owing to local buckling deformation are illustrated in Fig. 6(a). When the web-to-flange width ratio χ_f is

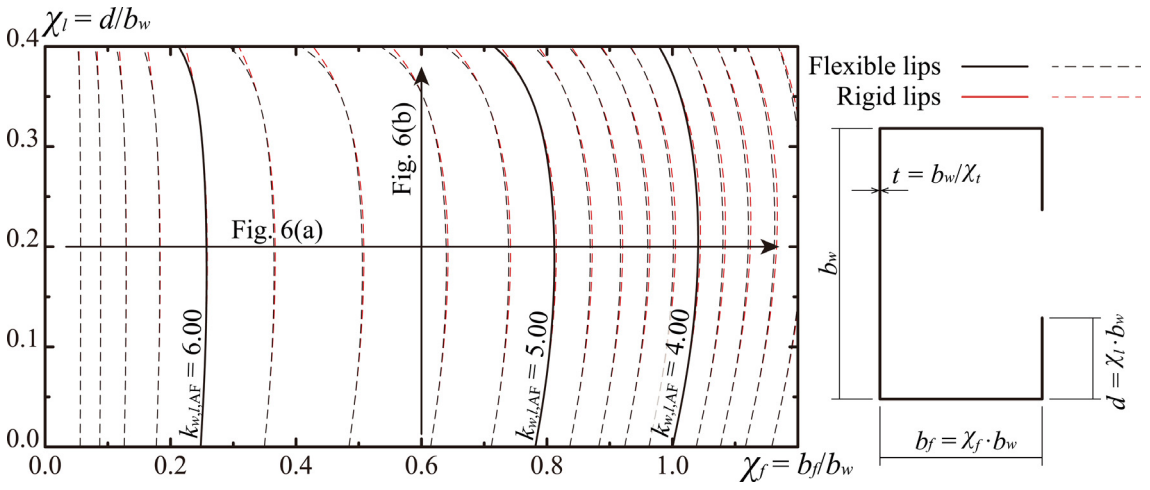

Fig. 5. Changes in the buckling coefficients for elastic critical local buckling according to geometric parameters $\chi_f = b_f/b_w$ and $\chi_l = d/b_w$. (For interpretation of the references to color in this figure legend, the reader is referred to the web version of this article.)

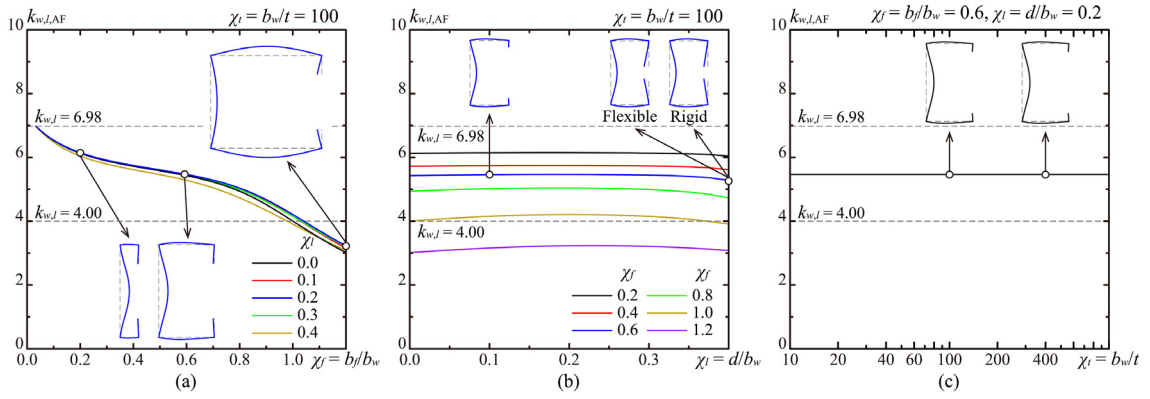

Fig. 6. Influence of cross-sectional geometry on buckling coefficient for local buckling: (a) $k_{w,l}$ vs. $\chi_f = b_f/b_w$. (b) $k_{w,l}$ vs. $\chi_l = d/b_w$. (c) $k_{w,l}$ vs. $\chi_t = b_w/t$.

small, the local buckling deformation around the junctures between the web and flanges hardly rotates and the buckling coefficient of the web is close to 6.98, indicating that the web experiences local buckling under the near-fixed-support condition. When the web-to-flange width ratio χ_f increases, the junctures between the web and flanges rotate; when it exceeds 1.0, the buckling coefficient of the web declines below 4.0, indicating that the local buckling of the flange determines the buckling load of the member. In this study, the plate element interaction is reflected in the elastic critical local buckling stress. Therefore, the local buckling stress of the member can be directly evaluated by the buckling coefficient of the web, even in cases where the local buckling of the flanges determines the elastic critical local buckling stress. Second, it can be concluded that the influence of the lip width on the buckling coefficient is not significant, as shown in Figs. 5 and 6(b). The difference between the results that account for lip flexibility and those that ignore the out-of-plane lip deflection is small when the web-to-lip width ratio $\chi_l = d/b_w$ is greater than 0.35. However, the extent to which the difference manifests itself is limited, and the cross-sectional deformations due to local buckling are almost identical, as shown in Fig. 6(b). The effect of the width-to-thickness ratio of the web, $\chi_t = b_w/t$, on the buckling coefficient is shown in Fig. 6(c). Eq. (18) does not include a variable for the width-to-thickness ratio; therefore, the buckling coefficient of the web does not change even if the width-to-thickness ratio changes, as shown in Fig. 6(c).

4. General formula for elastic critical local buckling

4.1. Estimation of elastic critical local buckling coefficient

In the practical design of the CFOS, the elastic critical local buckling stress of a member is determined by comparing or summarizing the elastic local buckling stress of each plate, which is obtained from Eq. (1). Although the buckling coefficient k in Eq. (1) varies for plates comprising the cross-section or their boundary conditions, the minimum value of the buckling coefficient obtained under the assumption of simply supported plates is used. In contrast, the buckling coefficient $k_{w,l}$ derived using the proposed analytical formula (Eq. (17)) is obtained as the buckling coefficient of the web and is directly converted from the elastic critical local buckling stress. In other words, the elastic critical local buckling stress of a member can be estimated by substituting $k_{w,l}$ obtained using Eq. (17) into Eq. (19).

$$\sigma_{cr,l} = k_{w,l} \frac{\pi^2 E t^2}{12\left(1-\nu^2\right) b_w^2} \tag{19}$$

Thus, the proposed design method is simple and enables a more accurate estimation of the local buckling stress when compared to the current design methods because the proposed analytical formula considers the plate element interaction. However, the proposed analytical formula requires computation to determine the minimum buckling coefficient, and its expression is complex. Hence, we simplified the

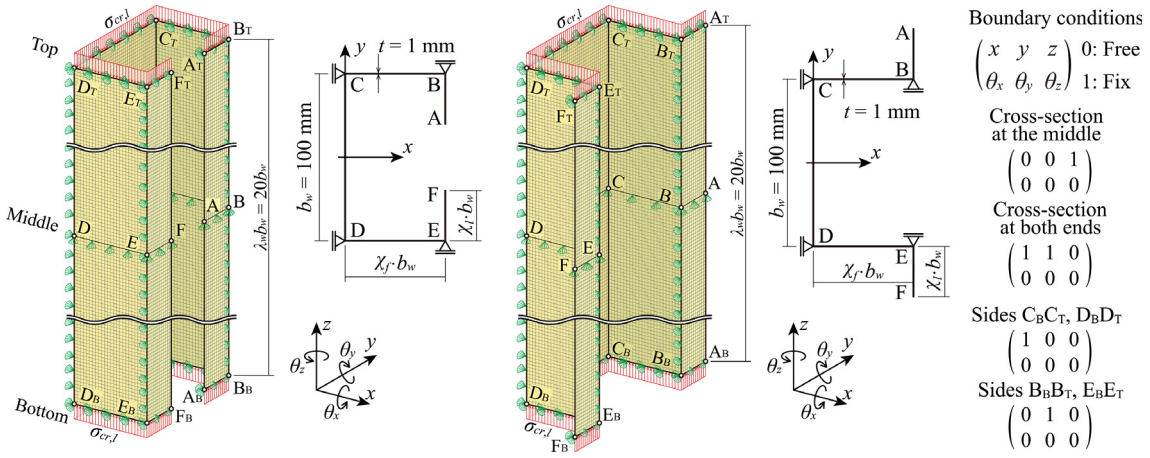

Fig. 7. FE models of CFOSs.

proposed analytical formula derived in Section 2 to obtain a novel general formula for calculating the minimum elastic critical local buckling stress of the CFOS based on the results of the parametric investigation described in Section 3 to make it easy for engineers to use. The parametric investigation results of the minimum elastic critical local buckling stress indicate that the buckling coefficient of the web for elastic critical local buckling was affected only by the web-to-flange width ratio χ_f and web-to-lip width ratio χ_l, and χ_f was the dominant variable. Based on the parametric investigation results, the buckling coefficient of the web for CFOS can be fitted using Eq. (20).

$$k_{w,l,\mathrm{P}} = \begin{cases} \chi_f\left(5.48\chi_f - 6\right) + 6.98 & 0.0 < \chi_f \le 0.5 \\ \chi_f\left\{-3.8\chi_f - 10\left(\chi_f - 0.5\right)\left[\left(\chi_l - 0.2\right)^2 - 0.04\right] + 3\right\} + 4.8 & 0.5 < \chi_f \le 1.2 \end{cases} \tag{20}$$

To investigate the reliability of the simplified formula in Eq. (20) and the analytical formula shown in Eq. (17), a parametric eigenvalue elastic buckling analysis based on FEA was performed. Fig. 7 illustrates the features of the FE model. The general FEA software MSC Marc version 2021 [27] was used to create a numerical model of the CFOS, as shown in Fig. 7. The FE model was constructed using Element 139 (four-node shell elements with six degrees of freedom at each node, with translations and rotations about three reference axes), which was suitable for analyzing thin-shell structures. To determine the appropriate mesh size, an eigenvalue analysis was conducted for different mesh sizes. Based on the results of the convergence study, a mesh size of (2.5 × 2.5 mm) was selected. For the material properties, the modulus of elasticity E was set to 205 GPa, and the Poisson's ratio ν was set to 0.3. For the models with the simply supported condition, the rotational degrees of freedom for the plate's end edges were removed, whereas the translational degrees of freedom in the x and y directions were restrained. The translational degrees of freedom at the middle of the member in the z direction were restrained. Additionally, to prevent buckling modes other than local buckling, the translational degrees of freedom at sides C_BC_T and D_BD_T in the x direction and the translational degrees of freedom at sides B_BB_T and E_BE_T in the y direction were restrained. Axial loads were introduced at the nodes at the plate end edges to apply uniform compression. As analytical variables, the web-to-flange width ratio χ_f was varied in the range of 0.2 to 1.2, and the web-to-lip width ratio χ_l was varied in the range of 0.0 to 0.4. The variables used in the parametric study are summarized in Table 1. The web depth b_w, thickness t, and length-to-width ratio of the web λ_w were fixed at 100 mm, 1.0 mm, and 20, respectively. Parametric FEA was performed on 216 different cross-sections.

A comparison of the elastic critical local buckling stress values obtained based on the proposed analytical formula $\sigma_{cr,l,\mathrm{AF}}$ (Eq. (17)) and the elastic critical local buckling stress values obtained by FEM, $\sigma_{cr,l,\mathrm{FEM}}$, is shown in Fig. 8. Table 2 summarizes the parametric study results. As mentioned earlier, because the elastic critical local buckling stresses of the lipped channel and hat sections with the same dimensions were identical, the results for the lipped channel section are presented as examples in Fig. 8. It is seen that the analytical formula can well predict the values of $\sigma_{cr,l,\mathrm{FEM}}$, as shown in Fig. 8(a). The mean and standard deviation of the predicted values based on the analytical formula $\sigma_{cr,l,\mathrm{AF}}$ (Eq. (17)), with respect to the FEM values $\sigma_{cr,l,\mathrm{FEM}}$, were 1.021 and 0.01229, respectively, and no analytical case had a predicted error of 5% or more. Therefore, the proposed analytical formula is applicable in the range of $0.0 < \chi_f \le 1.2$ (web-to-flange width ratio) and $0.0 \le \chi_l \le 0.4$ (web-to-lip width ratio). Second, Fig. 8(b) shows the comparison of the elastic critical local buckling stresses obtained from FEM, $\sigma_{cr,l,\mathrm{FEM}}$, and the proposed simplified formula (Eq. (20)) $\sigma_{cr,l,\mathrm{P}}$. Fig. 8(b) also depicts the comparison of the prediction results obtained from the FEA with those obtained from Schafer's formula in [7] ($\sigma_{cr,l,\mathrm{S}}$) and the classical design approach [1,4,5] that considers the plates as simply supported ($\sigma_{cr,l,\mathrm{CD}}$). As shown in Fig. 8(b), the simplified formula proposed in this study can provide more accurate prediction results for the local buckling stress than those obtained from the classical design approach and Schafer's formula. The mean and standard deviation (S.D.) of the predicted values based on the simplified formula (Eq. (20)) with respect to the FEM values were 0.9990 and 0.01740, respectively, indicating that the simplified formula can predict the local buckling stress with almost the same accuracy as the analytical formula presented in Eq. (17). Note that Schafer's formula may yield negative buckling stresses when the web-to-flange width ratio χ_f is relatively low and the web-to-lip width ratio χ_l is high, such as when $\chi_f = 0.2$ and $\chi_l = 0.25$. However, cross-sectional geometries with negative buckling stresses are not utilized in reality; therefore, Schafer's formula does not interfere with practical usage. In addition, Schafer's formula is an approximation of the FSM results, and therefore, it can help predict the local buckling stresses more accurately than the classical design method. As shown in Fig. 8, if the plate element interaction is not

Table 1
Parameter settings for FEM and CUFSM.

Parameters	Range
Depth of web b_w	100 mm
Thickness	1.0 mm
Web-to-flange width ratio $\chi_f = b_f/b_w$	{0.1, 0.2, 0.3, 0.4, 0.5, 0.6, 0.7, 0.8, 0.9, 1.0, 1.1, 1.2}
Web-to-lip width ratio $\chi_l = d/b_w$	{0.00, 0.05, 0.10, 0.15, 0.20, 0.25, 0.30, 0.35, 0.40}

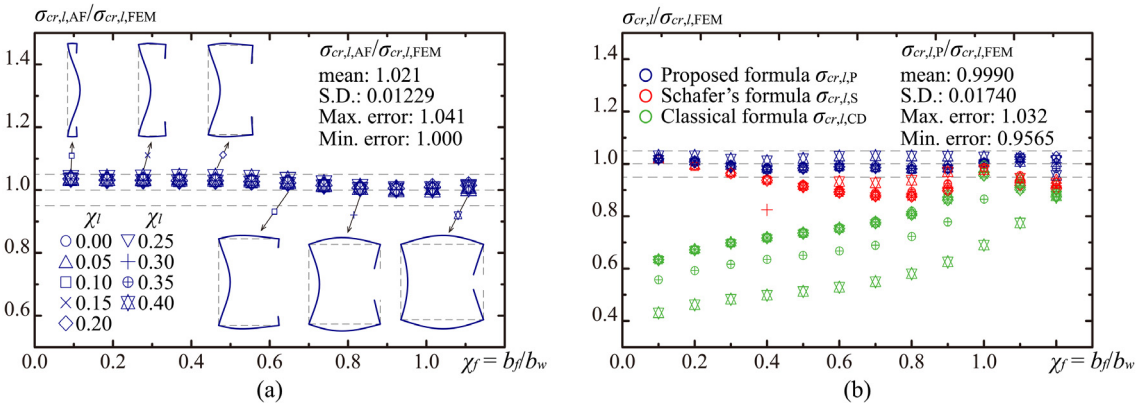

Fig. 8. Comparison of elastic critical local buckling stresses obtained from FEA and calculations: (a) Prediction results obtained from the analytical formula (Eq. (17)). (b) Prediction results obtained from the proposed simplified formula (Eq. (20)) and other design formulae.

Table 2
Comparison of the results of elastic critical local buckling stresses according to each method with the FEM results.

	$\sigma_{cr,l,AF}/\sigma_{cr,l,FEM}$	$\sigma_{cr,l,P}/\sigma_{cr,l,FEM}$	$\sigma_{cr,l,S}/\sigma_{cr,l,FEM}$	$\sigma_{cr,l,CD}/\sigma_{cr,l,FEM}$
Mean	1.021	0.9990	0.9246	0.7564
S.D.	0.01229	0.01740	0.03749	0.1247
Max.	1.041	1.032	1.016	0.9955
Min	1.000	0.9565	0.8246	0.4309

Note: The mean, standard deviation, maximum, and minimum of $\sigma_{cr,l,S}/\sigma_{cr,l,FEM}$ are obtained by excluding the results for which the predictions of Schaeffer's formula resulted in negative buckling stress.

correctly reflected in the design formula, the local buckling load of the CFOS will be significantly underestimated. Such a design method would lose the advantage of CFOS, which was developed for the advanced utilization of steel by varying the cross-sectional geometry. Therefore, design formulae that consider plate element interactions, such as the formulae proposed in this paper and Shaffer's formula, are essential to expand the usage of the CFOS.

4.2. Estimation of buckling half-wavelength that minimizes elastic critical local buckling stress

According to Timoshenko's plate buckling theory, the elastic critical buckling stress can be expressed using Eq. (16).

$$\sigma_{cr,l} = \frac{\Delta U_1 + 2\Delta U_2 + 2\Delta U_3}{\Delta T_1 + 2\Delta T_2 + 2\Delta T_3} \tag{21}$$

The critical half-wavelength ratio was obtained by substituting the eigenvalue vectors l_b, l_c, l_d, and l_f obtained from the analytical formula (Eq. (17)) into $\partial\sigma_{cr,l}/\partial\lambda_w = 0$. However, as mentioned previously, the proposed analytical formula requires computation. Therefore, the purpose of this subsection is to present novel general formulae for estimating the critical half-wavelength ratio that minimizes the elastic critical local buckling stress of the CFOS. It is well known that the critical half-wavelength ratios for the fixed and simply supported plates under uniform compression are 2/3 and 1.0 [1,5], respectively. In addition, the variation in the critical half-wavelength ratio is related to the changes in the buckling coefficient. Furthermore, the buckling coefficient of the web is affected by the web-to-flange width ratio χ_f and web-to-lip width ratio χ_l, where χ_f is the dominant variable. Therefore, the simplified formula for predicting the critical half-wavelength ratio of local buckling was proposed by fitting with χ_f and χ_l as the variables; the critical half-wavelength ratio λ_{cr} becomes 0.67 when $\chi_f = 0$ and $\chi_l = 0$, which was considered the fixed support condition, whereas it becomes 1.0 when $\chi_f = 1.0$ and $\chi_l = 0$, which was considered the simply supported condition.

(1) For $0.00 \le \chi_l \le 0.25$

$$\lambda_{cr,l,P} = \begin{cases} \chi_f/4 + 2/3 & 0.0 < \chi_f \le 0.8 \\ 2\chi_f/3 + 1/3 & 0.8 < \chi_f \le 1.2 \end{cases} \tag{22a}$$

(2) For $0.25 < \chi_l \le 0.40$

$$\lambda_{cr,l,P} = \begin{cases} \chi_f\left(0.75 + \chi_l\right)/4 + 2/3 & 0.0 < \chi_f \le 0.8 \\ \left[\chi_f\left(1.5 + 2\chi_l\right) + 1.25 - \chi_l\right]/3 & 0.8 < \chi_f \le 1.2 \end{cases} \tag{22b}$$

A comparison of the signature curves for local buckling and the proposed simplified formulae (Eqs. (20) and (22)) are shown in Fig. 9(a). For the material properties, the modulus of elasticity E was set to 205 GPa and Poisson's ratio ν was set to 0.3. The boundary condition of both ends was set to the simply supported condition in the CUFSM. As shown in Fig. 9(a), the proposed simplified formulae can predict the elastic critical local buckling stresses and critical half-wavelength ratio that minimizes the local buckling stress. Fig. 9(b) presents a comparison of the critical half-wavelength ratio for local buckling based on the proposed formula (Eq. (22)), $\lambda_{cr,P}$, and the critical half-wavelength ratio obtained by CUFSM, $\lambda_{cr,CUFSM}$. The variables for the parametric study were the same as those used in the FEM, as shown in Fig. 7. The mean and standard deviations of the predicted values based on the simplified formula (Eq. (22)) with respect to the CUFSM values were 0.9949 and 0.02069, respectively. Analytical cases with a prediction error of 5% or more were limited to χ_l greater than 0.40.

5. Conclusion

In this study, a series of displacement functions that can express the buckling deformations of the web, flanges, and lips, caused by local buckling in a CFOS, was developed by considering the effects of plate element interaction. Based on these displacement functions, a novel analytical formula for local buckling was derived, and the influence of cross-sectional geometry on the elastic critical local buckling load was investigated. The simplified formulae for the buckling coefficient and half-wavelength that minimize the elastic critical local buckling load were also presented for practical purposes. The validity of these formulae was demonstrated by comparing their results with the prediction results obtained through FEM and CUFSM. The following main conclusions were obtained:

(1) The analytical equation (Eq. (17)) accurately estimated the elastic critical local buckling stress and local buckling deformation of the CFOS.
(2) The buckling coefficient of the elastic critical local buckling of the CFOS was determined by the changes in the three shape

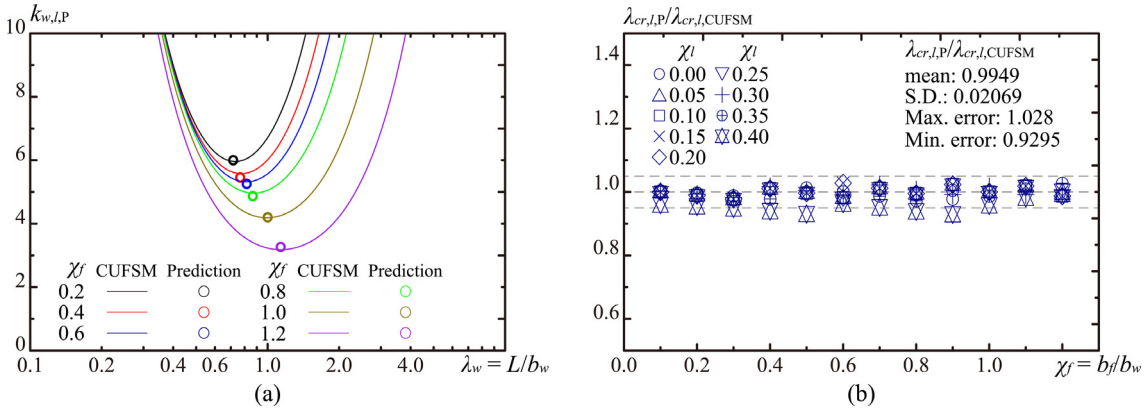

Fig. 9. Comparison of half-wavelengths for local buckling obtained from CUFSM with those calculated using the proposed formulae. (b) Prediction results obtained from the proposed simplified formulae (Eq. (22)).

factors [length-to-width ratio of the web ($\lambda_w = L/b_w$), web-to-flange width ratio ($\chi_f = b_f/b_w$), and web-to-lip width ratio ($\chi_l = d/b_w$)]. With an increase in the value of λ_w, the buckling coefficient converges to the minimum buckling coefficient. It was clear that the web-to-flange width ratio χ_f was the dominant factor for the minimum buckling coefficient for local buckling, whereas the influence of the web-to-lip width ratio was not significant.

(3) The validity of the proposed analytical equation (Eq. (17)) was verified by comparing it with the parametric eigenvalue elastic buckling analysis based on the FEM. The proposed analytical formula is applicable in the range of $0.0 < \chi_f \leq 1.2$ and $0.0 \leq \chi_l \leq 0.4$. The mean and standard deviation of the predicted values based on the analytical formula $\sigma_{cr,l,AF}$ with respect to the FEM values $\sigma_{cr,l,FEM}$ were 1.021 and 0.01229, respectively, and no analytical case had a prediction error of 5% or more.

(4) A simplified formula (Eq. (20)) was derived based on an analysis of the influence of cross-sectional geometry on the buckling stresses. The mean and standard deviation of the predicted values based on the simplified formula for the FEM values were 0.9990 and 0.01740, respectively, indicating that the simplified formula could predict the local buckling stress with almost the same accuracy as the analytical formula proposed in this study.

Notation

b	Width of the plate
b_w, b_f, d	Web depth, flange width, lip width
D	Flexural rigidity of the plate
E, ν	Modulus of elasticity and Poisson's ratio, respectively
k	Buckling coefficient
$k_{w,l}$	Buckling coefficient of the web for elastic critical local buckling of the CFOS
$k_{w,l,AF}$	Buckling coefficient of the web, determined using Eq. (17)
$k_{w,l,P}$	Buckling coefficient of the web, determined by the simplified formula presented in Eq. (20)
L	Member length
l_a, l_b, l_c, l_d	Constants that determine the cross-sectional deformation
m	Number of buckling half-waves along the longitudinal direction
t	Thickness of the plate
σ_0	Base stress defined in Eq. (15) to simplify the expression
σ_{cr}	Elastic critical buckling stress
$\sigma_{cr,l}$	Elastic critical local buckling stress
$\sigma_{cr,l,AF}$	Elastic critical local buckling stress of the CFOS, determined using Eq. (17)
$\sigma_{cr,l,CD}$	Elastic critical local buckling stress obtained from the classical design approach [1,4,5] that considers the plates as simply supported
$\sigma_{cr,l,FEM}$	Elastic critical local buckling stress obtained from the FEM analysis results
$\sigma_{cr,l,S}$	Elastic critical local buckling stress of the CFOS, determined by Schafer's formula in [7]
ΔU_1, ΔU_2, ΔU_3	Strain energy of a single plate for the web, flange, and lip, respectively.
ΔT_1, ΔT_2, ΔT_3	Work done by uniform compression on a single plate of the web, flange, and lip, respectively
Π	Potential energy
$\lambda_{cr,CUFSM}$	Critical half-wavelength ratio for local buckling, obtained using CUFSM software
$\lambda_{cr,P}$	Critical half-wavelength ratio for local buckling based on the proposed formula (Eq. (22))
λ_w	Length-to-width ratio of web (= L/b_w)
χ_f	Web-to-flange width ratio (= b_f/b_w)
χ_l	Web-to-lip width ratio (= d/b_w)
χ_t	Width-to-thickness ratio of web (= b_w/t)

CRediT authorship contribution statement

Kazuya Mitsui: Writing – original draft, Visualization, Validation, Supervision, Methodology, Funding acquisition, Formal analysis, Conceptualization. **Kikuo Ikarashi:** Writing – review & editing, Supervision, Methodology, Funding acquisition. **Tomoki Kobashi:** Writing – review & editing, Project administration, Methodology, Investigation. **Ryohei Kuwada:** Writing – review & editing, Visualization, Methodology, Investigation, Formal analysis.

Declaration of competing interest

The authors declare that they have no known competing financial interests or personal relationships that could have appeared to influence the work reported in this paper.

Data availability

Data will be made available on request.

Acknowledgments

This paper is supported by the Japan Society for the Promotion of Science, KAKENHI Grant (No. 20K14868 and No. 20H02294).

Appendix. Development of the theoretical procedure

Substituting Eqs. (2a), (4), (7) into Eqs. (9) and (12), each term related to the web is calculated as follows.

$$\int_0^L\int_0^{b_w}\left(\frac{\partial^2 w_w}{\partial y^2}\right)^2 dy dz = \int_0^L u(z)^2\,dz \cdot \frac{\pi^4}{b_w^3}\left(8l_b^2+\frac{l_c^2}{2\chi_f^2}+\frac{2l_d^2}{\chi_f^2}-\frac{16l_bl_c}{3\pi\chi_f}-\frac{32l_bl_d}{3\pi\chi_f}+\frac{2l_cl_d}{\chi_f^2}\right) \tag{A.1}$$

$$\int_0^L\int_0^{b_w}\left(\frac{\partial^2 w_w}{\partial z^2}\right)^2 dy dz = \int_0^L u''(z)^2\,dz \cdot b_w\left(\frac{3l_b^2}{2}+\frac{l_c^2}{2\chi_f^2}+\frac{2l_d^2}{\chi_f^2}-\frac{16l_bl_c}{3\pi\chi_f}-\frac{32l_bl_d}{3\pi\chi_f}+\frac{2l_cl_d}{\chi_f^2}\right) \tag{A.2}$$

$$\int_0^L\int_0^{b_w}\frac{\partial^2 w_w}{\partial y^2}\frac{\partial^2 w_w}{\partial z^2}dy dz = \int_0^L u(z)\,u''(z)\,dz \cdot \frac{\pi^2}{b_w}\left(-2l_b^2-\frac{l_c^2}{2\chi_f^2}-\frac{2l_d^2}{\chi_f^2}+\frac{16l_bl_c}{3\pi\chi_f}+\frac{32l_bl_d}{3\pi\chi_f}-\frac{2l_cl_d}{\chi_f^2}\right) \tag{A.3}$$

$$\int_0^L\int_0^{b_w}\left(\frac{\partial^2 w_w}{\partial y\partial z}\right)^2 dy dz = \int_0^L u'(z)^2\,dz \cdot \frac{\pi^2}{b_w}\left(2l_b^2+\frac{l_c^2}{2\chi_f^2}+\frac{2l_d^2}{\chi_f^2}-\frac{16l_bl_c}{3\pi\chi_f}-\frac{32l_bl_d}{3\pi\chi_f}+\frac{2l_cl_d}{\chi_f^2}\right) \tag{A.4}$$

$$\int_0^L\int_0^{b_w}\left(\frac{\partial w_w}{\partial z}\right)^2 dy dz = \int_0^L u'(z)^2\,dz \cdot b_w\left(\frac{3l_b^2}{2}+\frac{l_c^2}{2\chi_f^2}+\frac{2l_d^2}{\chi_f^2}-\frac{16l_bl_c}{3\pi\chi_f}-\frac{32l_bl_d}{3\pi\chi_f}+\frac{2l_cl_d}{\chi_f^2}\right) \tag{A.5}$$

Substituting Eqs. (2b) and (5) into Eqs. (10) and (13), the terms related to the flange and web are calculated as follows.

$$\int_0^L\int_0^{b_f}\left(\frac{\partial^2 w_f}{\partial x^2}\right)^2 dx dz = \int_0^L u(z)^2\,dz \cdot \frac{\pi^4}{b_w^3\chi_f^3}\left(\frac{l_c^2}{2}+1.89l_d^2+0.770l_cl_d\right) \tag{A.6}$$

$$\int_0^L\int_0^{b_f}\left(\frac{\partial^2 w_f}{\partial z^2}\right)^2 dx dz = \int_0^L u''(z)^2\,dz \cdot b_w\chi_f\left(\frac{l_c^2}{2}+\frac{0.378l_d^2}{\chi_f^2}+0.770l_cl_d\right) \tag{A.7}$$

$$\int_0^L\int_0^{b_f}\frac{\partial^2 w_f}{\partial x^2}\frac{\partial^2 w_f}{\partial z^2}dx dz = \int_0^L u(z)\,u''(z)\,dz \cdot\left[-\frac{\pi^2}{b_w\chi_f}\left(\frac{l_c^2}{2}+0.639l_d^2+0.770l_cl_d\right)\right] \tag{A.8}$$

$$\int_0^L\int_0^{b_f}\left(\frac{\partial^2 w_f}{\partial x\partial z}\right)^2 dx dz = \int_0^L u'(z)^2\,dz \cdot \frac{\pi^2}{b_w\chi_f}\left(\frac{l_c^2}{2}+0.639l_d^2+0.770l_cl_d\right) \tag{A.9}$$

$$\int_0^L\int_0^{b_f}\left(\frac{\partial w_f}{\partial z}\right)^2 dx dz = \int_0^L u'(z)^2\,dz \cdot b_w\chi_f\left(\frac{l_c^2}{2}+\frac{0.378l_d^2}{\chi_f^2}+0.770l_cl_d\right) \tag{A.10}$$

Substituting Eqs. (2c), (6), and (8) into Eqs. (11) and (14), each term related to the lip is calculated as follows:

$$\int_0^L\int_0^{d}\left(\frac{\partial^2 w_l}{\partial y^2}\right)^2 dy dz = \int_0^L u(z)^2\,dz \cdot \frac{\pi^4 l_f^2}{32b_w^3\chi_l^3} \tag{A.11}$$

$$\int_0^L\int_0^{d}\left(\frac{\partial^2 w_l}{\partial z^2}\right)^2 dy dz = \int_0^L u''(z)^2\,dz \cdot b_w\chi_l\left[\frac{\pi^2\chi_l^2l_c^2}{3\chi_f^2}+\frac{(3\pi-8)\,l_f^2}{2\pi}+\frac{\left(\pi^2-4\pi+8\right)\chi_l l_c l_f}{\pi\chi_f}\right] \tag{A.12}$$

$$\int_0^L\int_0^{d}\frac{\partial^2 w_l}{\partial y^2}\frac{\partial^2 w_l}{\partial z^2}dy dz = \int_0^L u(z)\,u''(z)\,dz \cdot \frac{\pi}{b_w\chi_f}\left[\frac{(4-\pi)\,\chi_f l_f^2}{8\chi_l}+\frac{(\pi-2)\,l_c l_f}{2}\right] \tag{A.13}$$

$$\int_0^L\int_0^{d}\left(\frac{\partial^2 w_l}{\partial y\partial z}\right)^2 dy dz = \int_0^L u'(z)^2\,dz \cdot \frac{\pi^2}{b_w\chi_f}\left(\frac{\chi l_c^2}{\chi_f}+\frac{\chi_f l_f^2}{8\chi_l}+\frac{2l_cl_f}{\pi}\right) \tag{A.14}$$

$$\int_0^L\int_0^{d}\left(\frac{\partial w_l}{\partial z}\right)^2 dy dz = \int_0^L u'(z)^2\,dz \cdot b_w\chi_l\left[\frac{\pi^2\chi_l^2l_c^2}{3\chi_f^2}+\frac{(3\pi-8)\,l_f^2}{2\pi}+\frac{\left(\pi^2-4\pi+8\right)\chi_l l_c l_f}{\pi\chi_f}\right] \tag{A.15}$$

$u(z)$, $u'(z)$, and $u''(z)$ in Eqs. (A.1)–(A.15) are the displacement functions in the longitudinal direction depending on the boundary conditions at both ends of the plates. Substituting Eqs. (3a) or (3b) into $u(z)$, $u'(z)$, and $u''(z)$, the following equations for the simply and fixed support condition can be obtained:

(1) For simply supported condition

$$\int_0^L u(z)^2\,dz = \frac{L}{2} \tag{A.16}$$

$$\int_0^L u''(z)^2\,dz = \left(\frac{m\pi}{L}\right)^4\frac{L}{2} \tag{A.17}$$

$$\int_0^L u(z)\,u''(z)\,dz = -\left(\frac{m\pi}{L}\right)^2\frac{L}{2} \tag{A.18}$$

$$\int_0^L u'(z)^2\,dz = \left(\frac{m\pi}{L}\right)^2\frac{L}{2} \tag{A.19}$$

(2) For fixed support condition

$$\int_0^L u(z)^2\,dz = \frac{L}{4} \tag{A.20}$$

$$\int_0^L u''(z)^2\,dz = \left(\frac{\pi}{L}\right)^4\frac{\left[4m^2+\left(m^2+1\right)^2\right]L}{4} \tag{A.21}$$

$$\int_0^L u(z)\,u''(z)\,dz = -\left(\frac{\pi}{L}\right)^2\frac{\left(m^2+1\right)L}{4} \tag{A.22}$$

$$\int_0^L u'(z)^2\,dz = \left(\frac{\pi}{L}\right)^2\frac{\left(m^2+1\right)L}{4} \tag{A.23}$$

References

[1] North American Specification (NAS) for the Design of Cold-Formed Steel Structural Members - AISI S100-12-C, American Iron and Steel Institute (AISI), Washington, D.C., 2020.
[2] B.W. Schafer, Review: The direct strength method of cold-formed steel member design, J. Construct. Steel Res. 64 (7–8) (2008) 766–778.
[3] S. Ádány, B.W. Schafer, A full modal decomposition of thin-walled, single-branched open cross-section members via the constrained finite strip method, J. Construct. Steel Res. 64 (1) (2008) 12–29.
[4] Cold-Formed Steel Structures AS/NZS 4600:2018, Standards Australia, Sydney, Australia, 2005.

[5] Guide for Designing Cold-Formed Steel Structures, 2nd ed., Gihodo Shuppan Co., Ltd., Tokyo, Japan, 2014.
[6] B.W. Schafer, T. Peköz, Laterally braced cold-formed steel flexural members with edge stiffened flanges, ASCE J. Struct. Eng. 125 (2) (1999) 118–127.
[7] B.W. Schafer, Local, distortional, and Euler buckling of thin-walled columns, ASCE J. Struct. Eng. 128 (3) (2002) 289–299.
[8] T. Kobashi, K. Ikarashi, N. Shimizu, Elastic local buckling strength and maximum strength of cold formed steel members with different plate width on adjacent plate elements, Jpn. Archit. Rev. 2 (4) (2019) 465–476.
[9] T. Kobashi, K. Ikarashi, N. Shimizu, Elastic local buckling strength and maximum strength of rectangular section members which were loaded compression and bending, J. Struct. Constr. Eng. (Trans. AIJ) 84 (755) (2019) 97–107, (In Japanese).
[10] C. Yu, B.W. Schafer, Stress gradient effect on the buckling of thin plates, in: 17th International Specialty Conference on Cold-Formed Steel Structures, 2004, pp. 47–69.
[11] Y. Kimura, S.M. Fujak, A. Suzuki, Elastic local buckling strength of I-beam cantilevers subjected to bending moment and shear force based on flange–web interaction, Thin-walled Struct. 162 (2021) 107633.
[12] K. Mitsui, K. Ikarashi, Buckling strength and behavior of elastic local buckling for cold-formed channel member under compression, J. Struct. Constr. Eng. (Trans. AIJ) 86 (790) (2021) 1685–1692, (In Japanese).
[13] G.C. de Salles, E. de M. Batista, D.C.T. Cardoso, A modal decomposition approach for experimental buckling analysis of thin-walled lipped channel columns, Eng. Struct. 256 (2022) 113979.
[14] Y. Lu, W. Li, T. Zhou, H. Wu, Novel local buckling formulae for cold-formed C-section columns considering end condition effect, Thin-walled Struct. 116 (2017) 265–276.
[15] T. Zhou, Y. Lu, W. Li, H. Wu, End condition effect on distortional buckling of cold-formed steel columns with arbitrary length, Thin-walled Struct. 117 (2017) 282–293.
[16] V. Piluso, A. Pisapia, G. Rizzano, Local buckling of aluminium channels under uniform compression: Theoretical analysis and experimental tests, Thin-walled Struct. 179 (2022) 109511.
[17] H.T. Nguyen, S.E. Kim, Buckling of composite columns of lipped-channel and hat sections with web stiffener, Thin-walled Struct. 47 (2009) 1149–1160.
[18] Y.B. Kwon, B.S. Kim, G.J. Hancock, Compression tests of high strength cold-formed steel channels with buckling interaction, J. Constr. Steel Res. 65 (2) (2009) 278–289.
[19] S. Jin, Z. Li, T. Gao, F. Huang, D. Gan, R. Cheng, Constrained shell finite element method of modal buckling analysis for thin-walled members with curved cross-sections, Eng. Struct. 240 (1) (2021) 112281.
[20] M.V.A. Kumar, V. Kalyanaraman, Design strength of locally buckling stub-lipped channel columns, J. Struct. Eng. 138 (11) (2012) 1291–1299.
[21] S. Li, O. Zhao, Local buckling and capacity of press-braked ferritic stainless steel channel sections under minor-axis combined loading, Thin-walled Struct. 178 (2022) 109507.
[22] Y.B. Kwon, G.J. Hancock, Tests of cold-formed channels with local and distortional buckling, J. Struct. Eng. 118 (7) (1992) 1786–1803.
[23] H. Debski, A. Teter, T. Kubiak, S. Samborski, Local buckling, post-buckling and collapse of thin-walled channel section composite columns subjected to quasi-static compression, Thin-Walled Struct. 136 (2016) 593–601.
[24] L. Huang, W. Yang, T. Shi, J. Qu, Local and distortional interaction buckling of cold-formed thin-walled high strength lipped channel columns, Int. J. Steel Struct. 21 (2021) 244–259.
[25] S.P. Timosenko, J.M. Gere, Theory of Elastic Stability, 2nd ed., McGraw-Hill Book Inc., New York, 1961.
[26] B.W. Schafer, CUFSM5.04-Finite Strip Buckling Analysis of Thin-Walled Members, Baltimore, Department of Civil Engineering, Johns Hopkins University, U.S.A., 2020, http://www.ce.jhu.edu/bschafer/cufsm/.
[27] MSC Software Corporation, Marc Version 2020 Volume A–D, MSC Software Corporation, 2021.